Mathematical Model of the Hydrocyclone Based on Physics of Fluid Flow

K. T. Hsieh and R. K. Rajamani
Comminution Center, University of Utah, Salt Lake City, UT 84112

A mathematical model of the hydrocyclone, based on the physics of fluid flow, has been developed. The model equations are solved in a computer code that takes as input the hydrocyclone dimensions and feed slurry characteristics. The output of the computer code is the velocity profiles of the fluid and the separation efficiency curve. To validate the model, an LDV was used to measure the velocity profiles inside a 75-mm hydrocyclone. Pure water and glycerol-water mixture were used as the working media to simulate the increase of slurry viscosity in the presence of solid particles. The predicted velocity profiles agree well with the experimental measurements. Dilute limestone slurry was also classified with the same hydrocyclone, and predicted the separation efficiency curve shows good agreement with experimental observation.

Introduction

Hydrocyclones are used widely in the chemical, mineral and powder-processing industries. They consist of a cylindrical section with a central tube (Figure 1) connected to a conical section with a discharge tube. An inlet tube is attached to the top section of the cylinder in such a way that it is tangential to the cylinder at the point of entry. Another variation of the inlet design is the involute entry used commonly in mineral slurry applications. The fluid being injected tangentially into the hydrocyclone causes swirling within the device, thus generating centrifugal force. In this centrifugal field, coarser and heavier particles move toward the wall and are swept downward to the spigot. The conical section constricts the downward spiraling flow, and hence a central column of liquid is spiraling upward and exits via the vortex finder. The upward flow carries with it finer and lighter particles.

The swirling fluid flow is a classic fluid mechanics problem, which can be analyzed with the Navier-Stokes equations. Extensive efforts on modeling of swirling flows have been devoted by the combustion community (Syred and Beér, 1974; Lilley, 1977; Sloan et al., 1986). The difficulties, however, are that the current system comprises multiple phases—liquid, air, and solid particles (each particle size or density represents an additional phase) and that the swirling flow is turbulent. The objective of this study is to model the hydrocyclone in this manner to predict the particle separation efficiency curve. The unique aspect of modeling with the Navier-Stokes equations is that, in the numerical solution, the geometry of the hydrocyclone is implicitly accounted for, and hence the validated model is useful for the design of hydrocyclones in specific applications.

The hydrocyclone fluid-flow problem has been the subject of few investigations since the 1940's. A number of earlier works focused on studying the fluid-flow patterns and suggested highly simplified theories to explain the flow (Kelsall, 1952; Ohashi and Maeda, 1958; Bradley and Pulling, 1959; Lilge, 1962; Knowles et al., 1973; Dabir and Petty, 1984; Gu and Li, 1987). Over the years, the Navier-Stokes equations gradually crept into the model equations with a number of oversimplifying assumptions (Driessen, 1951; Rietema and Krajenbrink, 1959; Rietema, 1961, 1962; Bhattacharyya, 1980; Laverack, 1980; Upadrashta et al., 1987). In a series of publications, Bloor and Ingham (1973, 1975a, 1975b, 1987) manipulated the Navier-Stokes equations to answer some aspects of the hydrocyclone fluid-flow problem. To date the most successful work in predicting the fluid flow in the hydrocyclone is that of Rhodes et al. (1987). They used the PHOENICS computer code for the solution of partial differential equations involved. With a modified Prandtl mixing-length model and the symmetry assumption, their velocity predictions of a 200-mm hydrocyclone were excellent. This work, however, did not validate the model for variations of geometry or feed conditions.

Correspondence concerning this article should be addressed to K. T. Hsieh.

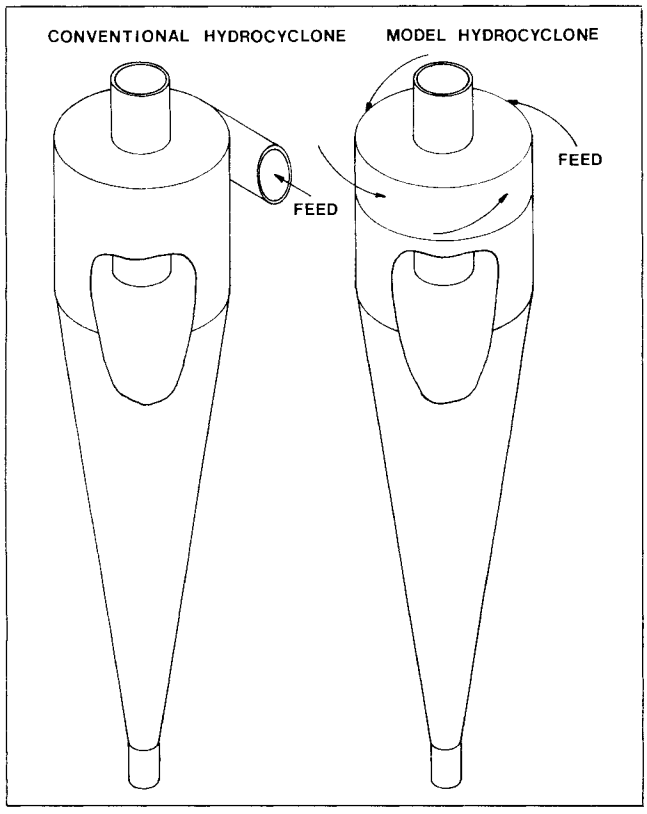

Figure 1. Isometric view of conventional and modeled hydrocyclones.

Table 1. Dimensions of the Experimental Hydrocyclone

Diameter of the hydrocyclone	75	mm
Diameter of the tangential inlet	25	mm
Diameter of the vortex finder	25	mm
Diameter of the spigot	12.5	mm
Length of the vortex finder	50	mm
Length of the cylindrical section	75	mm
Included cone angle	20°	

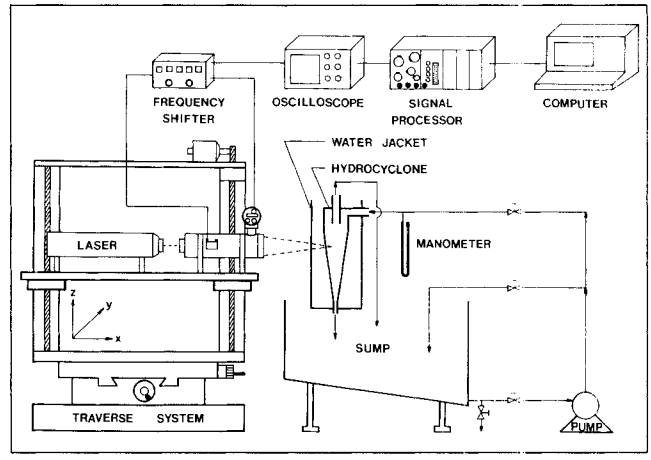

Figure 2. Hydrocyclone and laser-Doppler velocimeter system.

Experimental Work

The experimental work was divided into two tasks: liquid-phase velocity profile measurements and particle-size classification experiments. The velocity measurement rig consisted of a hydrocyclone, a pump, a sump, an LDV and a three-dimensional traverse assembly. A schematic drawing of this rig is shown in Figure 2. In this study a single-channel dual-beam, 35-mW He-Ne laser-Doppler velocimeter was used. Since the air core blocked the scattered light as it passed through the liquid/air interface, the backscatter alignment was chosen. The frequency shifter permitted the detection of flow direction as well as the measurement of low-velocity flow. The dimensions of the 75-mm glass hydrocyclone used in the experimental work are listed in Table 1. The thickness of the glass wall was 1 mm throughout. During the experiments, the hydrocyclone was immersed in a water-filled jacket made of 6-mm-thick Plexiglas plate to minimize the optical refraction of the laser beams.

It is not possible to measure velocities in opaque fluids with the LDV system; hence, alternate fluids that would simulate slurries were sought. Both water and glycerol are Newtonian fluids. The viscosity of food-grade glycerol is around 1,300 to 1,400 cp (1.3 to 1.4 Pa·s). When mixed with water, the viscosity of the mixture decreases exponentially with the increase in water content. Therefore, water and a glycerol-water mixture were used as the fluid media in these experiments. Seeding the fluid to increase the data rate is common practice in laser-Doppler velocimetry. In these experiments, 1.5-μm silicon carbide particles seemed to work well. The tangential velocity component was measured at two opposite vertical planes, while the axial velocity component was measured at four vertical planes 90° apart. Since the air core fluctuates at all times, the radial velocity could not be measured accurately with the current LDV system. The tangential velocity component being two orders of magnitude higher than the radial velocity component overwhelmed the latter in the viewing direction of the laser beams. However, this quantity can be computed with the continuity equation using measured axial and tangential velocities.

The particle-size classification experiment was conducted in a standard sump-pump recirculation system. A dilute limestone slurry was prepared and pumped through the same 75-mm glass hydrocyclone. Both underflow and overflow streams were sampled, and the size distribution was determined by a Microtrac particle-size analyzer. The operating conditions of the velocity profile measurements and the size classification experiment are listed in Table 2.

Experimental Results and Discussion

The experimental velocity profiles offer some qualitative observations. The axial velocity profiles for series I and II are plotted in Figures 3 and 4, respectively. The profiles are asymmetric about the vertical axis in the vortex finder region, because the inlet flow enters on one side of the vertical axis only. This asymmetry is predominant near the region where the inlet flow enters and gradually becomes almost symmetric below the vortex finder. However, asymmetry appears again in the vicinity of the spigot, since the fluid-flow passage narrows, giving rise to an unstable pressure field, which in turn causes the air core to fluctuate.

Table 2. Experimental Operating Conditions

Series No.	I	II	III
Viscosity (kg/m·s)	0.001	0.01	0.00113
Suspension Composition	Water	1:1 Glycerol-Water	10.47 wt. % Limestone
Solid (kg/min)	—	—	8.21
Feed			
Liquid (kg/min)	66.99	74.60	70.24
Solid (kg/min)	—	—	4.58
Overflow			
Liquid (kg/min)	63.72	67.00	67.21
Solid (kg/min)	—	—	3.63
Underflow			
Liquid (kg/min)	3.27	7.60	3.03

Interestingly enough, there is more than one reversal in flow direction in the region between the vortex finder and the wall. This observation is contrary to the commonly-held belief that there is a single envelope that separates the upward-directed flow in the central region from the downward-directed flow near the wall. As the fluid enters the hydrocyclone tangentially, linear momentum of the inlet flow is transformed into angular momentum, and the main stream flows toward the spigot. When the fluid moves into the conical section, it is restricted by the narrow cone; hence, a central upward spiraling flow is introduced. It is the interaction of this upward flow with the main downward stream that causes multiple flow reversals. The flow reversal would depend on the cone angle as well as the ratio of the diameter of the vortex finder to that of the hydrocyclone. For very high inlet flows, multiple flow reversal zones can appear even in the conical part.

The short-circuiting phenomenon, wherein part of the feed stream travels down the outer wall of the vortex finder and merges with the upward flow, is known in the literature (Bloor and Ingham, 1975b; Heiskanen et al., 1987, Hsieh and Rajamani, 1988). Direct evidence of short-circuiting is found in the axial velocity profiles shown in Figures 3 and 4. In both

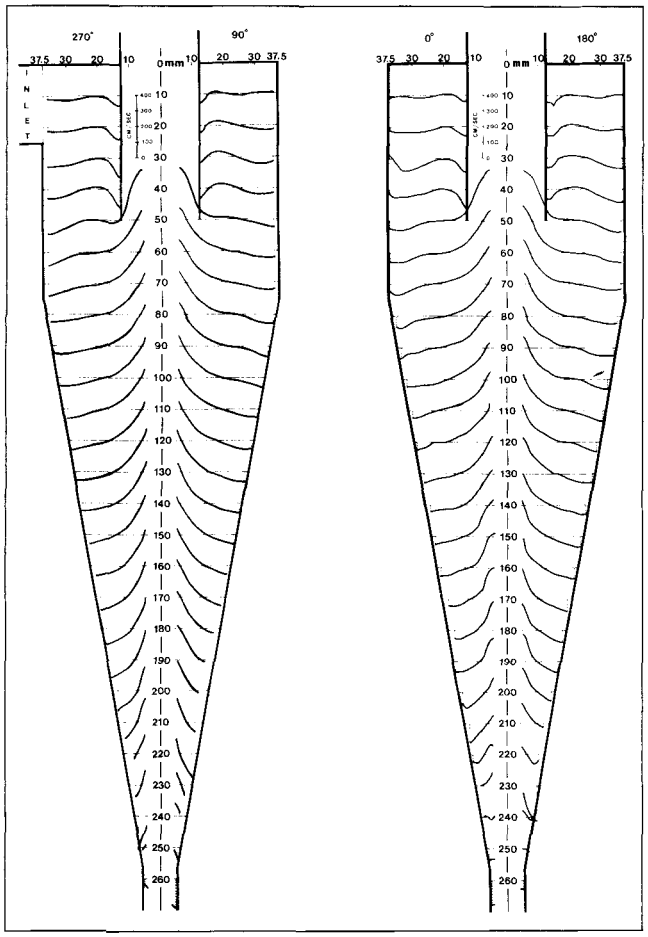

Figure 3. Axial velocity profile for series I (water only) measured by LDV.

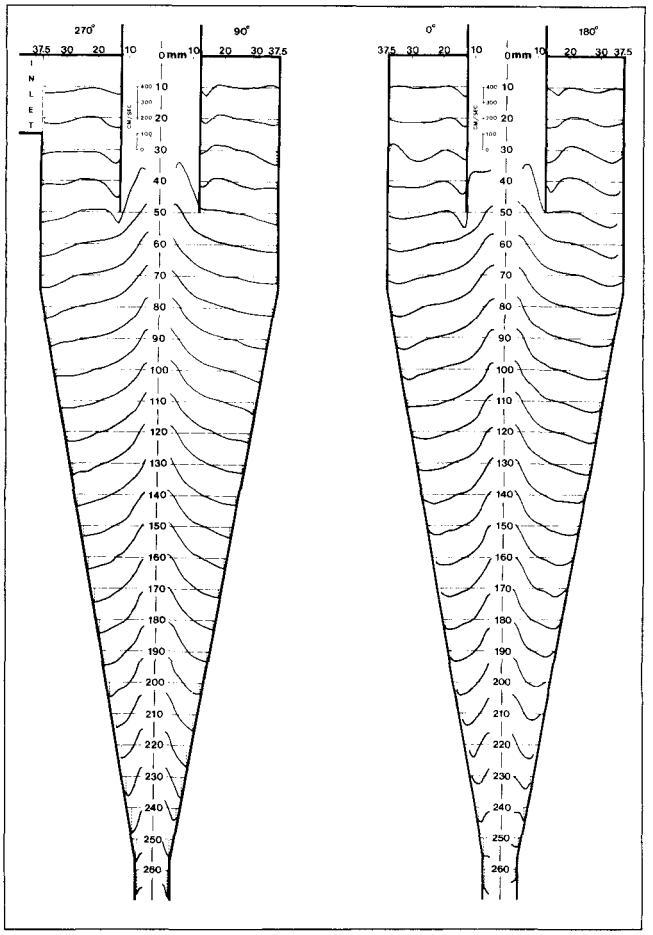

Figure 4. Axial velocity profile for series II (glycerol-water mixture) measured by LDV.

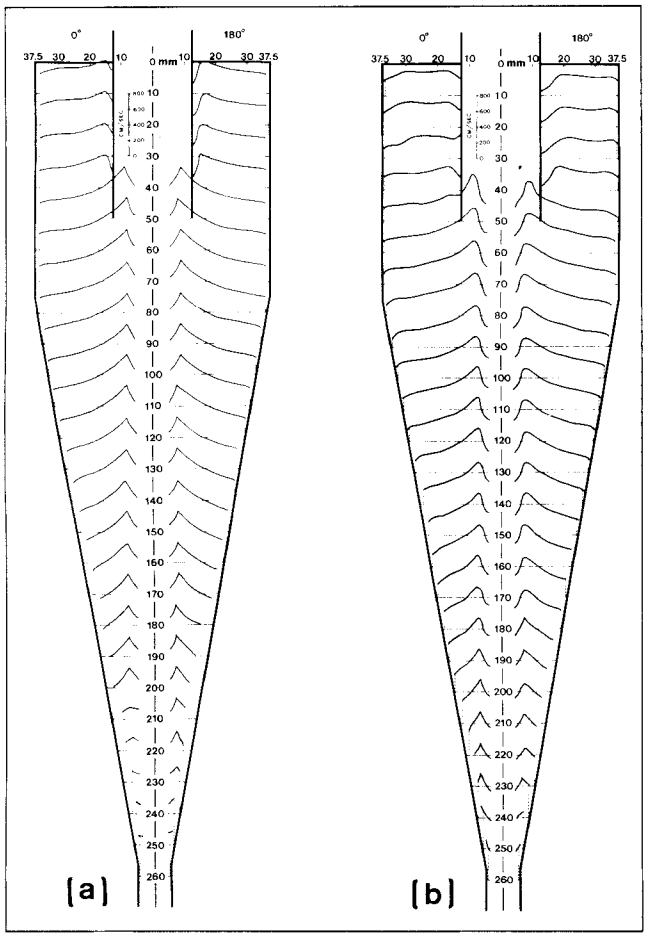

Figure 5. Tangential velocity profiles measured by LDV: (a) series I (water only); (b) series II (glycerol-water mixture).

series, the flow moves downward along the outer wall of the vortex finder; however, the magnitude depends on the inlet flow rate. Short-circuiting is a mechanism by which a portion of the feed stream leaves unclassified and thus to which the inefficiency of the device is attributed. Short-circuiting flow is most pronounced at the back side of the tangential inlet (270° angle as seen in Figures 3 and 4) and it increases with the increase of fluid viscosity. Another noticeable feature is that the axial flow reverses along most parts of the hydrocyclone except at regions very close to the spigot, and consequently very little fluid discharges through the underflow.

The tangential or spinning velocity component generates the centrifugal force, which separates coarser particles from finer ones. The tangential velocity profiles for series I and II are shown in Figure 5. The forced vortex can be seen in the central region adjacent to the air core, and the free vortex prevails thereafter. Here, too, asymmetry is observed in the upper vortex finder region, though not as pronounced as in the axial velocity profiles. Below the vortex finder, envelopes of constant tangential velocity are cylinders coaxial within the hydrocyclone.

In the conical section, the shape of the tangential velocity profile is very similar throughout the region; also, the slope of the forced vortex is nearly the same. This is due to the tapering of the conical section, which compensates for the dissipation of momentum due to friction in that region. For the same mean inlet velocity, the peak tangential velocity decreases with the increase in viscosity. Finally, a noticeable feature of both experimental series is that, even though the operating conditions are different, the trends are similar in both axial and tangential velocity profiles.

Modeling of the Fluid Flow

Complete modeling work of the hydrocyclone involves predicting the liquid-phase velocities, the slurry concentration profile, the turbulent viscosities, the slip velocities of particles with respect to the liquid phase, and finally the particle separation efficiency curve of the device. The problem becomes complex, because the governing fluid-flow equations are nonlinear, simultaneous partial differential equations, and adding to this complexity is the presence of liquid, air and solid phases within the hydrocyclone. A full multiphase approach will not be pursued, as it would be difficult to keep computer time reasonable. In view of the fact that particle slip velocities in the hydrocyclone are likely to be small, alternatively, we assume that particle-fluid momentum coupling is absent and thus break the modeling work into two parts. First, the liquid-phase fluid-flow problem is solved to predict the liquid-phase velocities; then, the particle motion with respect to the fluid is computed by balancing all forces acting on the particle itself. We postulate that, if we can calculate the velocities of particles with respect to the fluid, then the trajectories of particles of each size, from their entry into the unit until their exit via one of the outlets, can be predicted, which in turn yields the particle separation curve of the hydrocyclone.

Strictly speaking, the modeling work of liquid-phase velocities and particle motion within the hydrocyclone are interdependent, because the liquid-phase velocities are affected by local density and viscosity, which are functions of solid concentration as well as particle-size distribution of the slurry, and the particle motion determines the slurry concentration profile and the particle-size distribution at each location. For a dilute slurry where the variations of local density and viscosity are small and particle/particle interactions are negligible, the computation of liquid-phase velocities and particle motion can be executed independently. For a concentrated slurry, however, the computation of liquid-phase velocities and particle motion has to be set in an iterative mode so that the changes of local density and viscosity due to particle motion will be estimated, and this information will then be used to recompute liquid-phase velocities. It should also be noted that particle/particle interactions become more significant for concentrated slurries and could affect the separation efficiency of the hydrocyclone. For instance, the misplacement of fine particles to the underflow stream could be attributed to the blockage of their movement toward the axis of symmetry by the presence of coarse particles; and the misplacement of coarse particles to the overflow stream could be ascribed to the re-entrainment due to the inability of the spigot opening to cope with the excessive number of particles that have been swept downward.

Assumptions

Since the LDV-measured velocity profiles are generally ax-

isymmetric in the azimuthal direction everywhere except in the regions close to the inlet and the outlets, axisymmetry is naturally assumed for this modeling work. While single-tube entry causes the asymmetry in the inlet region, the short-circuiting flow and the narrow passage area are responsible for the asymmetry in the vicinity of the vortex finder and the spigot, respectively. Nevertheless, the velocities in the main body of the hydrocyclone determine particle classification and these profiles are axisymmetric. Therefore, the assumption of axisymmetry is justified.

The assumption of axisymmetry implies that the single-inlet flow has to be distributed in some manner to obtain appropriate initial conditions for this two-dimensional model. It is then decided here, as in Brayshaw (1978), to model the inlet flow through a full 360° inlet ring instead of the single tangential entry tube. The assumed ring inlet, shown in Figure 1, allows the same volumetric flow to enter. This hypothetical ring inlet would, of course, be extremely difficult to construct in practice. However, this is not important as far as the model is concerned. What is important is that the ring inlet approximates very closely the conventional mode of single-tube entry, in principle and in outcome. It is believed that the fluid entering through the tangential inlet will distribute itself around the cylindrical section, and the ring inlet approximates this condition.

Transport equations

Although it is possible to numerically solve the governing Navier-Stokes equations written in primitive variables, many successful solutions have utilized the vorticity-stream function approach (Roache, 1972). For two-dimensional incompressible turbulent flow with constant properties and no body forces, the dimensionless modeled transport equations written in conservative form relative to cylindrical coordinates are (Hsieh, 1988) as follows.

Vorticity:

$$\frac{\partial \eta}{\partial t}=\frac{1}{r^3}\frac{\partial \Omega^2}{\partial z}-\frac{\partial u\eta}{\partial r}-\frac{\partial w\eta}{\partial z}+\frac{1}{Re}\left(\frac{\partial^2\eta}{\partial r^2}+\frac{1}{r}\frac{\partial \eta}{\partial r}-\frac{\eta}{r^2}+\frac{\partial^2\eta}{\partial z^2}\right) \tag{1}$$

Stream function:

$$\frac{\partial^2\Psi}{\partial r^2}-\frac{1}{r}\frac{\partial \Psi}{\partial r}+\frac{\partial^2\Psi}{\partial z^2}=-r\eta \tag{2}$$

Angular spin velocity:

$$\frac{\partial \Omega}{\partial t}=-\frac{\partial u\Omega}{\partial r}-\frac{u\Omega}{r}-\frac{\partial w\Omega}{\partial z}+\frac{1}{Re}\left(\frac{\partial^2\Omega}{\partial r^2}-\frac{1}{r}\frac{\partial \Omega}{\partial r}+\frac{\partial^2\Omega}{\partial z^2}\right) \tag{3}$$

and

$$\frac{1}{r}\frac{\partial \Psi}{\partial r}=w,\quad -\frac{1}{r}\frac{\partial \Psi}{\partial z}=u,\quad \frac{\Omega}{r}=v, \tag{4}$$

where Re is the Reynolds number defined as R_cU_o/ν. It should be noted that the normalization constant used here is based on the advective time scale R_c/U_o, where R_c is the hydrocyclone radius and U_o is the mean inlet velocity, and that the axisymmetry assumption implies that all derivatives in the azimuthal direction are set to zero.

Turbulent transport

The correlation between the turbulence and the Reynolds number has not been established for vortical flow, yet it is generally believed that turbulent conditions exist within the body of the hydrocyclone, especially since the inlet Reynolds number is as high as 10^5 to 10^6 for most practical applications. Excellent reviews on currently available models for calculating turbulent stresses are abundant in the literature (Rodi, 1982; Sloan et al., 1986). Generally speaking, more comprehensive turbulence models are formulated on the basis of two separate viewpoints. The first perspective assumes that an isotropic eddy viscosity and the modified Boussinesq hypothesis adequately describe the stress distributions and that the source of predictive error is a consequence of the modeled terms in the κ-ϵ equations. A second viewpoint proposes that the eddy viscosity approach is inherently inadequate and that a redistribution of the stress magnitudes is necessary. This infers the use of higher-order closure schemes based on transport equations for the Reynolds stresses. However, models employing transport equations for the Reynolds stresses constitute a large number of differential equations, whose solution is not a trivial task. Hence, algebraic stress closures have been developed by simplifying the differential transport equations to algebraic expressions but retaining most of their basic features. Since it is the convection and diffusion terms that make the transport equations differential equations, these terms need to be simplified by model approximations.

The use of a κ-ϵ turbulence model in its standard form is unrealistic for the current system since anisotropy is imposed on the flow by high swirling stresses (Pericleous et al., 1984). A better model would be the algebraic stress model proposed by Boysan et al. (1982). However, it is felt that this model is too complicated and time-consuming. In addition, it does not take into account the effect of the presence of the solid particles on the properties of the fluid. Experimental results show that effective viscosity of the slurry in the hydrocyclone increases rapidly with the increase of solid concentration. The Prandtl mixing-length hypothesis is one of the first turbulence models proposed, and interestingly is still among the most widely used models. It employs the eddy viscosity/diffusivity concept, which relates the turbulent transport terms to the gradients of mean-flow quantities. For two-dimensional boundary-layer flow, particularly those developing over rigid boundaries, the mixing-length hypothesis combines a good mixture of accuracy and simplicity. Because the flow pattern of the hydrocyclone indicates that the axial velocity gradient in the radial direction is of the same order of magnitude compared to the tangential velocity gradient in that direction, a modified Prandtl mixing-length model is proposed for this modeling effort which reads:

$$\mu_t=\rho_m\lambda^2\left(\left|\frac{\partial V}{\partial R}-\frac{V}{R}\right|+\left|\frac{\partial W}{\partial R}\right|\right) \tag{5}$$

The proposed turbulence model takes into account the effect of the presence of solid particles on the turbulence of the fluid by assuming a slurry density that depends on solid concentra-

tion, and a turbulent viscosity that in turn depends on the slurry density and viscosity. Equation 5 involves a single unknown parameter, the mixing length λ, which is a characteristic length scale of the turbulent motion and whose distribution over the flow field has to be prescribed with the aid of empirical information. Pericleous et al. (1984) used a fraction of the hydrocyclone radius as the mixing length with success. However, we consider that the mixing length varies both radially and axially inside the hydrocyclone and that separate expressions of the mixing length should be prescribed for swirling and nonswirling components (Okhio et al., 1986; Morsi and Clayton, 1986). A number of correlations were examined in this investigation; the best ones that compare favorably with experimental velocity data are the following:

$$\lambda_\eta = 0.010 R_c \left(\frac{\mu_m}{\mu_o}\right)^{1/5} \left(\frac{R_z}{R_c}\right)^{1/4} \left(\frac{R}{R_c}\right)^{1/2} \tag{6}$$

$$\lambda_\Omega = 0.015 R_c \left(\frac{\mu_m}{\mu_o}\right)^{1/5} \left(\frac{R_z}{R_c}\right)^{1/4} \left(\frac{R}{R_c}\right)^{1/2} \tag{7}$$

where R_z is the radius of the hydrocyclone at the horizontal level under consideration, μ_m is the viscosity of the slurry, and μ_o is the viscosity of water.

Boundary conditions

The boundaries where steady-state conditions should be specified are the inlet and outlets (vortex finder and spigot), the solid wall, and the liquid/air interface (air core). The inlet conditions are known beforehand; therefore, a mass inflow of liquid and concentration of solid are preset at the beginning of the computation. Conditions at the outlets of the hydrocyclone are not known, and zero-gradient conditions are applied on the assumption that the flow has become more or less fully developed when it reaches the exit plane. At both outlets, the solution domain is best extended beyond the hydrocyclone body to preserve the rotational characteristics of the flow. The value of angular-spin velocity at the wall is approximated by a logarithmic wall function in lieu of fine grid calculations, and the LDV-measured tangential velocity profile is used to fine-tune this approximation. The boundary value of vorticity is more difficult to obtain and is an extremely important quantity. The vorticity transport equation for $\partial\eta/\partial t$ determines how η is advected and diffused. The total η is conserved at interior points, but at the no-slip boundary η is produced. Actually, it is the diffusion and subsequent advection of vorticity, which is produced at the wall that drives the problem. If Ψ_{w+1} is expanded by the Taylor series around the wall value Ψ_w and the no-slip condition is used, we get:

$$r\eta_w = -2\frac{\Psi_{w+1} - \Psi_w}{\Delta n^2} + O(\Delta n) \tag{8}$$

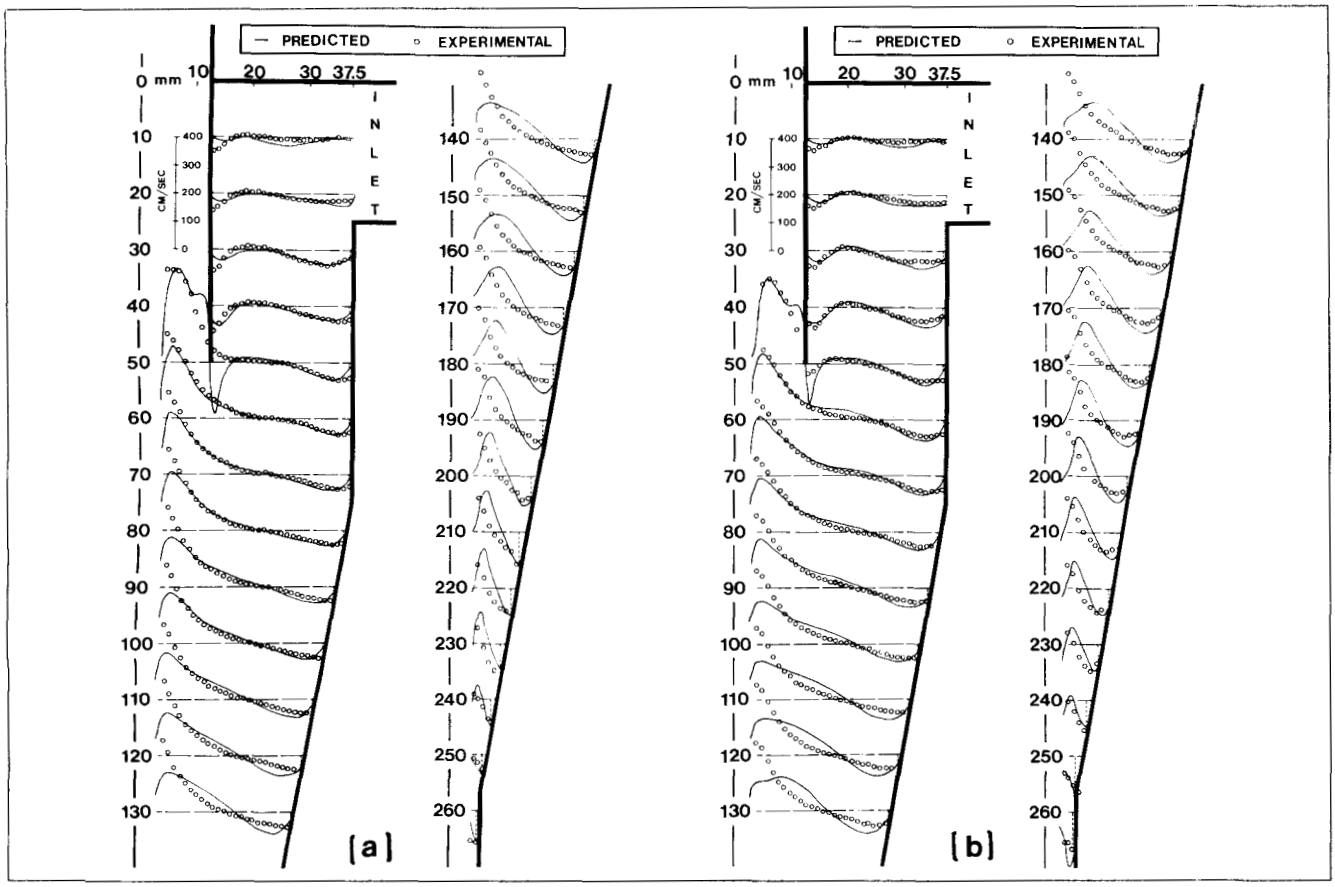

Figure 6. Measured and predicted axial velocity profiles: (a) series I (water only); (b) series II (glycerol-water mixture).

where Δn is the dimensionless distance from $(w+1)$ to w, normal to the wall.

The liquid/air interface, which divides the body of the fluid and the central column of air forming the air core itself, is impervious to the fluid and hence is represented by a stream surface. Although this stream surface corresponds to a constant Ψ, the value of Ψ is not specified but is free to develop as the computation proceeds; i.e., more and more fluid reverses its direction and exits through the vortex finder as the steady state is approached. The air core is parabolic in shape and has a larger radius in the vortex finder region than that in the vicinity of the spigot. Plausible formulations of the air-core radius for hydrocyclones with wide variations in design and operating variables are virtually nonexistent in the literature (Kelsall, 1952; Lilge, 1962; Tarjan, 1962). Iterative computation to achieve atmospheric pressure on the liquid/air interface could be devised if the model equations were formulated in primitive variables. In this modeling work, however, the air-core radius is determined to be the smallest value that still reaches a convergent numerical solution.

Numerical solution

The numerical problem on hand is a set of coupled parabolic and elliptic differential equations. Equations 1 and 3 are parabolic, and they pose an initial-value problem. These equations are solved using the Hopscotch method (Gourlay, 1970), where the solution is stepped out from some initial conditions. Equation 2 is elliptic, which poses a boundary-value problem, and is solved by the successive overrelaxation (SOR) method (Frankel, 1950; Young, 1954). A rectangular mesh system was adopted where small radial mesh size would be favored due to the high-velocity gradient in the radial direction. A small axial mesh size should be used in the vortex finder region to account for short-circuiting flow, while in the conical part, it was set in such a way that node points fall exactly on the conical wall. As far as the stability is concerned, the change in axial mesh spacing must be gradual so as not to deteriorate the formal order of truncation error. The computations were carried out on a SPARC workstation (SUN Microsystems), which required three hours of CPU time for approximately 2,000 iterations.

Predicted flow patterns

The Reynolds number of the inlet flow determines the velocity profiles: i.e., the momentum of the feed flow is distributed into tangential, axial and radial directions. As the model disregards the asymmetric flow, the averaged values of the velocity components measured at different vertical planes are compared with model predictions. Also, the radial component was not measured experimentally; therefore, only the model predictions are shown.

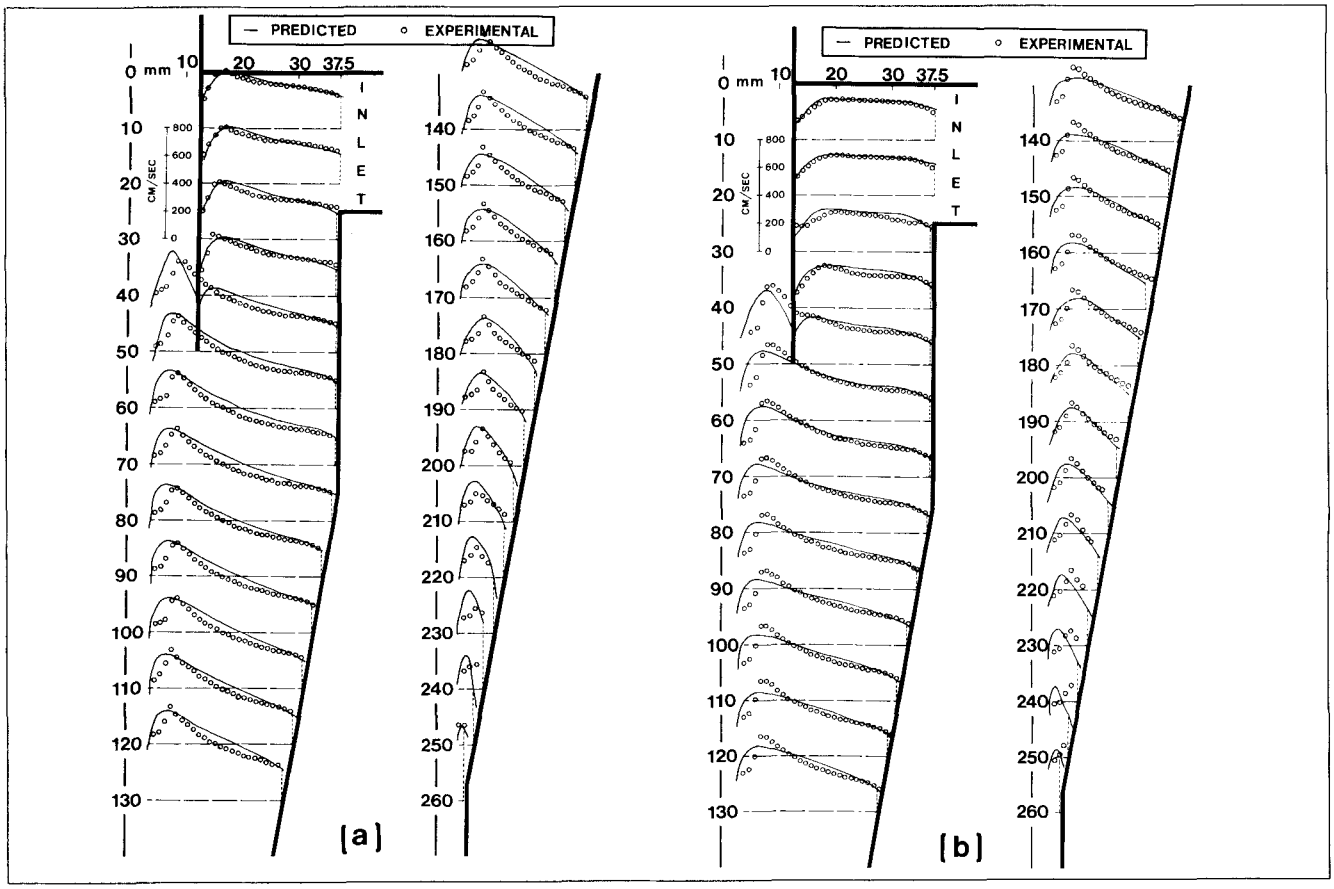

Figure 7. Measured and predicted tangential velocity profiles: (a) series I (water only); (b) series II (glycerol-water mixture).

The predicted and experimental axial velocity profiles for series I and II are compared in Figure 6. In the inlet and cylindrical section, the flow reversal and the magnitude of the axial flow are precisely predicted. The short-circuiting flow on the outer wall of the vortex finder is also well predicted, except at the tip of the vortex finder where the model seems to overpredict the downward flow. In the conical part, some discrepancies are observed. First, there is a consistent lateral shift of the locus of zero axial velocity. Secondly, the model predicts a thicker boundary at the liquid/air interface, which in turn varies the shape of the axial velocity profile in that region. It is noteworthy that the axial velocity should fall rapidly to zero when it reaches the liquid/air interface where the impermeability condition is applied. However, the current LDV system failed to measure the sharp velocity variation in this thin boundary layer due to the fluctuation of the air core. Incidentally, all the aforementioned discrepancies can be minimized or eliminated by using a very fine mesh system to solve the boundary-layer flow more elegantly at the expense of a much longer CPU time. In the vicinity of the spigot, close agreement is again observed, which ensures that the outflow through the spigot is predicted accurately.

In the modeling of highly swirling flow, it has been found that the correct prediction of the tangential velocity is essential to adequately reproduce the rest of the flow field. Indeed, tangential velocities are predicted accurately. The predictions for series I and II are shown in Figure 7. The experimentally observed forced-free vortex is predicted closely by the model. The peak velocities are also predicted accurately at each horizontal level with the exception of a few close to the spigot.

The radial velocity is the liquid "current," against which the particles must settle for them to be removed in the underflow; it is also the smallest of the three components. The predicted radial velocity profiles are plotted in Figure 8 for series I and II. A negative radial velocity means that the fluid is moving toward the axis of symmetry. The strong inward flow from the inlet to the vortex finder is readily seen in the top region. It gradually decreases and then reverses due to the central upward flow from the conical region meeting the hydrocyclone roof. Immediately below the vortex finder, there is an extremely strong inward flow, which accounts for the short-circuiting phenomenon. The steep rise of the radial velocity in that region is due to the strong downward flow along the outer wall of the vortex finder that reverses its direction in a very short distance as it exits through the vortex finder. In the conical portion, the inward radial velocity is small in the central region and increases to a maximum close to the wall.

Particle-Size Classification Prediction

The ultimate aim of the modeling effort is to predict the size classification brought about by the hydrocyclone. The general performance of the hydrocyclone is influenced both by such design variables as hydrocyclone dimensions, and operating variables as solid concentration, mass flow rate, and

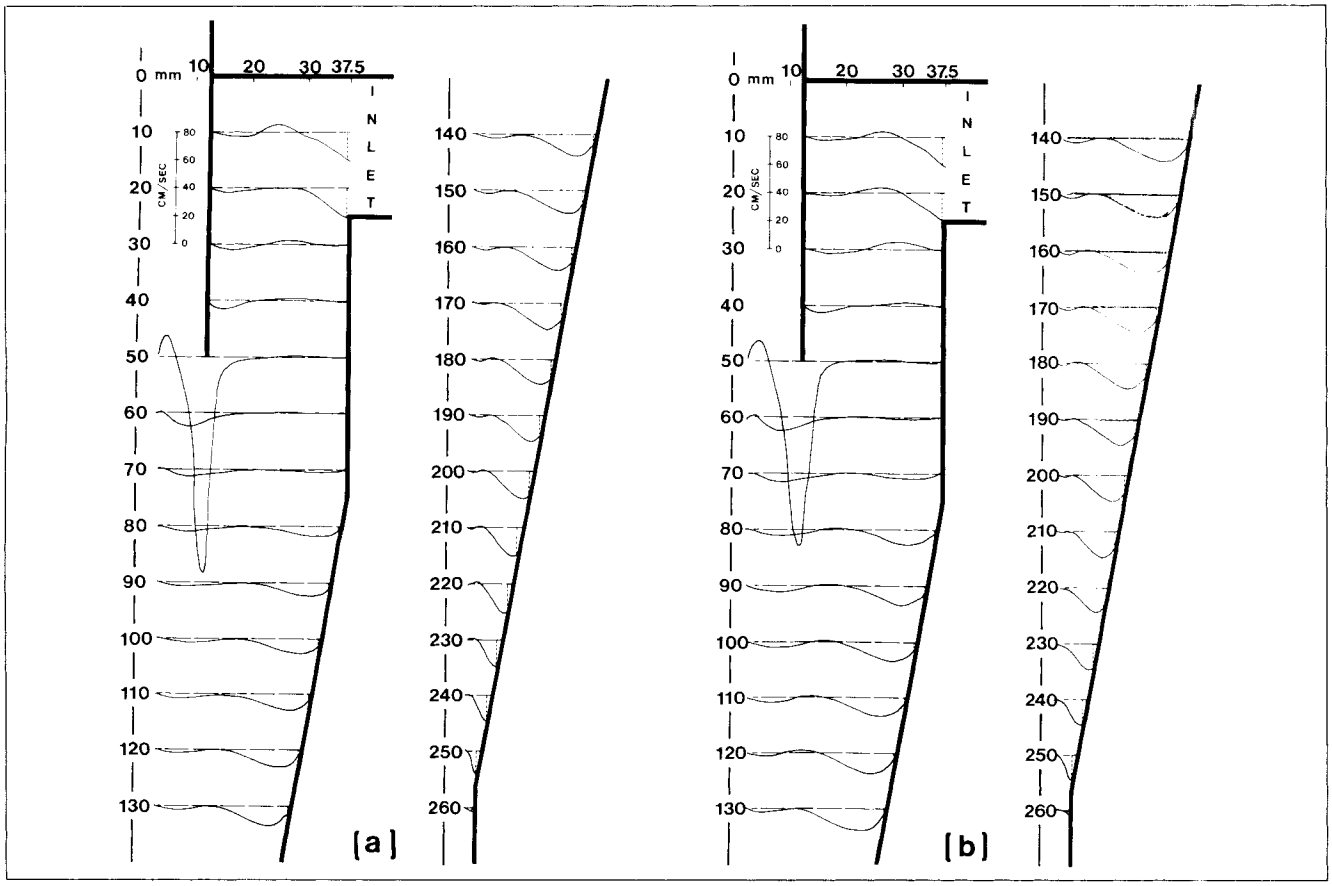

Figure 8. Predicted radial velocity profiles: (a) series I (water only); (b) series II (glycerol-water mixture)

particle-size distribution. The plot of fraction, or the percentage of each particle size of the feed reporting to the underflow discharge, vs. the particle size is called the "separation efficiency curve," and it is commonly used to describe the performance. To determine this curve, the trajectory of each particle must be tracked from the time it enters the hydrocyclone to the time it exits via one of the outlets. Depending on the size and density of the particle, it lags the fluid velocity. Therefore, the relative velocity must be determined before we can compute particle trajectories.

Particle slip velocities

Particle slip velocities are determined by a dynamic force balance on the particle itself. A single particle of diameter D_p and density ρ_p experiences two forces in the radial direction: the centrifugal force directed radially outward from the axis of symmetry and the radial drag force that opposes the centrifugal force. The forces in the axial direction are the gravitational force and the opposing drag force. As there are no significant forces acting on the particle in the tangential direction, it is considered to move along with the fluid in that direction.

By balancing the centrifugal force against the radial drag force we obtain:

$$(\rho_p - \rho_m)\frac{V^2}{R}\frac{\pi D_p^3}{6} = \frac{1}{2}\rho_l U_s^2 \frac{\pi D_p^2}{4} C_D \tag{9}$$

where

ρ_m = slurry density
ρ_l = fluid density
C_D = drag coefficient (Pericelous et al., 1984)

Equation 9 can be solved for the radial slip velocity, U_s,

$$U_s = \left|\frac{4}{3}\left(\frac{\rho_p - \rho_m}{\rho_l}\right)\frac{V^2}{R}\frac{D_p}{C_D}\right|^{1/2} \tag{10}$$

Similarly, by balancing the forces in the axial direction we obtain:

$$(\rho_p - \rho_m)g\frac{\pi D_p^3}{6} = \frac{1}{2}\rho_l W_s^2 \frac{\pi D_p^2}{4} C_D \tag{11}$$

Equation 11 is solved for the axial slip velocity, W_s,

$$W_s = \left|\frac{4}{3}\left(\frac{\rho_p - \rho_m}{\rho_l}\right) g\frac{D_p}{C_D}\right|^{1/2} \tag{12}$$

Particle trajectories

The trajectory of a particle depends on the location (across the diameter of the inlet tube) at which it enters the hydro-

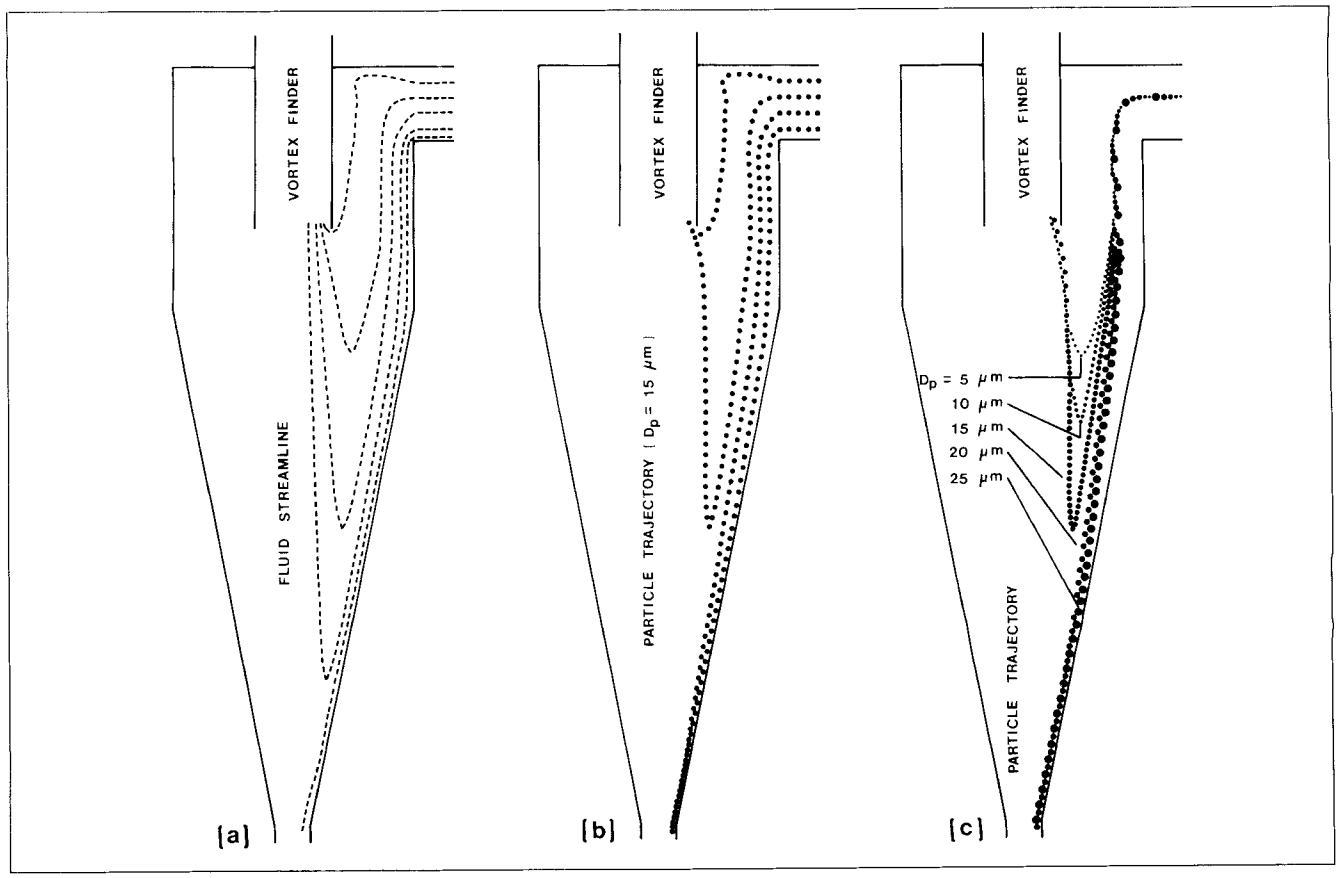

Figure 9. Computed trajectories of limestone particles for series I (water only): (a) fluid streamlines; (b) same particle size from different entry points; (c) different particle sizes from same entry point.

cyclone. It is assumed that the particles of any size are equally likely to enter at any location across the inlet tube, and the inlet tube is divided into 101 portions with equal spacing, so that there are 100 particle entry points excluding the two at the wall. Starting from each of the entry points the particle trajectory tracing procedure begins, and the particle displacement is calculated for a small time interval in both radial and axial directions. The computational routine is repeated until the particle leaves the hydrocyclone through either the vortex finder or the spigot.

The particle trajectories show the features of the hydrocyclone that have been either hypothesized or confirmed indirectly. The predicted streamlines for series I are shown in Figure 9a where most of the feed stream reports to the overflow. This is consistent with experimental results: i.e., 95% of the water reports to the overflow. The two boundary-layer flows are readily seen: first, a stream moves closer to the roof and then over the outer wall of the vortex finder; secondly, another stream moves along the cylindrical wall and then the conical wall. The first one joins the overflow stream and the second one goes to the underflow; these are streams that leave the hydrocyclone without being classified. Finally, one can see the feed streams that initially flow downward and then reverse their direction to join the overflow.

Figure 9b demonstrates the computed trajectories of a few 15-μm-dia. limestone particles emanating from different entry points for series I. By comparing Figure 9b with Figure 9a, the diverted particle trajectories from the fluid streamlines, due to radially and axially directed forces, are clearly seen. It is noted that, while a fluid stream reports to the overflow, a limestone particle starting from the same entry point could be classified and thus reports to the underflow.

The essence of the classification effect of the hydrocyclone is most clearly demonstrated in Figure 9c, where the trajectories of five different size limestone particles (5-μm to 25-μm-dia.) for series I are shown. After entering the hydrocyclone from the same entry point, all particles move downward along the cylindrical section and then into the conical section. Strong inward flow in the conical section brings the fine particles toward the axis of symmetry. These fine particles reverse their direction after passing their respective equilibrium orbits and move toward the vortex finder along with the central upward flow. As for the coarse particles, the large centrifugal force pushes them toward the conical wall despite the strong inward flow. Then they join the boundary-layer flow along the conical wall and exit through the spigot.

Particle classification curves

For a certain particle size in the feed stream, the particle trajectories are traced from each of the 100 entry points. The number of particle trajectories leading to the spigot discharge denotes the percentage of that particle size classified to the underflow. Repeating this procedure for all sizes yields the classification curve. It should be noted that, based on our experimental operating condition, particles are assumed to move through dilute slurries where particle/particle interactions are negligible.

The computed classification curves of limestone particles for series I and II are shown in Figure 10. It is seen that the cut size increases drastically from 15 μm to 78 μm as the fluid

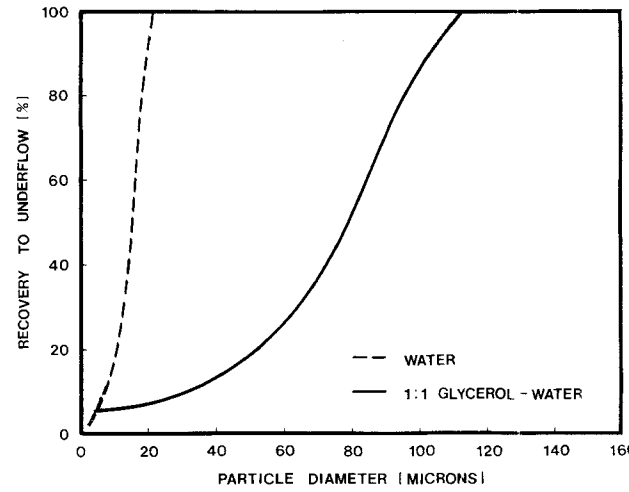

Figure 10. Predicted separation efficiency curves of limestone particles for series I (water only) and II (glycerol-water mixture).

viscosity increases from 1 cp to 10 cp (1 to 10 mPa·s). The effect here is attributed more to the variation of the drag force acting on the particles than to the minor change of the liquid-phase velocities as seen in Figures 6, 7 and 8. It is concluded that as the viscosity of the slurry increases there must be a tremendous increase of the drag force that alters the particle trajectories, increases the cutsize, and decreases the sharpness of separation.

Finally, the predicted and experimental classification curves for series III are compared in Figure 11. In this case, the general trend of the classification curve and the cut size are predicted very closely. A slight discrepancy is observed in the coarse size range, and the hypothetical ring inlet in the model formulation is believed to be responsible for this discrepancy. In the experimental hydrocyclone, the inlet radial velocity generated by a single tangential inlet tube is several times higher than that generated by the model's ring inlet. As a result, coarse particles

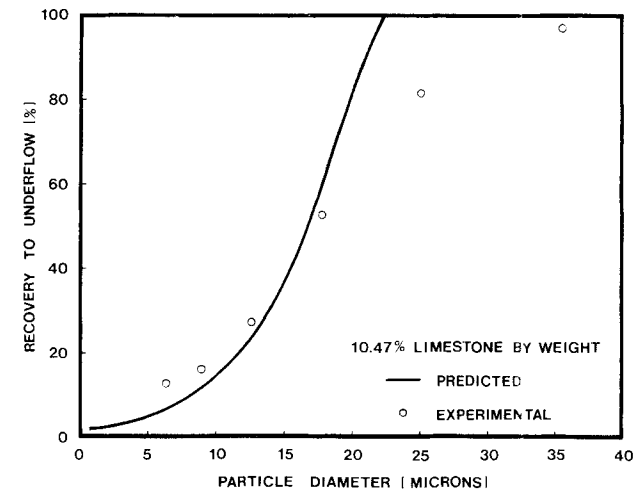

Figure 11. Measured and predicted separation efficiency curves for series III (limestone/water slurry).

have a higher probability of reaching the boundary-layer flow along the vortex finder outer wall and then short-circuiting to the overflow. In the model prediction, however, this short-circuiting effect has not been fully accounted for. Despite this shortcoming, the predictions are satisfactory, and furthermore the entire classification curve is predicted.

Conclusions

The governing Navier-Stokes equations have been solved successfully for the hydrocyclone geometry. The key to the success is the appropriate turbulence model and numerical solution scheme. A number of hydrocyclone runs at various operating conditions have confirmed the model predictions. The confirmation of the model for variations in hydrocyclone dimensions will appear in a future publication. Of course, refinement and validation of the model for handling primarily non-Newtonian behavior of slurries and particle/particle interactions are needed before it is used in hydrocyclone design. It appears that the basic construction of the model is sound and well justified.

Acknowledgment

This research has been supported by the Department of the Interior's Mineral Institute program administered by the Bureau of Mines through the Generic Mineral Technology Center for Comminution under grant number G1175149.

Notation

C_D = drag coefficient
D_p = diameter of a spherical particle, cm
g = gravitational acceleration, cm/s^2
Δn = dimensionaless distance from $(w+1)$ to w, normal to the wall, Eq. 8
R = radial distance from the axis of symmetry in cylindrical coordinates, cm
R_c = radius of the hydrocyclone, cm
Re = Reynolds number of the hydrocyclone defined as R_cU_o/ν
R_z = radius of the hydrocyclone at the horizontal level under consideration, cm
r = dimensionless radial distance from the axis of the symmetry in cylindrical coordinates
t = dimensionless time
U_o = mean inlet velocity, cm/s
U_s = particle radial slip velocity, cm/s
u = dimensionless radial velocity of the fluid
V = tangential velocity of the fluid, cm/s
v = dimensionless tangential velocity of the fluid
W = axial velocity of the fluid, cm/s
W_s = particle axial slip velocity, cm/s
w = dimensionless axial velocity of the fluid
z = dimensionless axial distance from the roof of the hydrocyclone in cylindrical coordinates

Greek letters

λ = Prandtl mixing length, cm
ρ_l = density of the fluid, g/cm^3
ρ_m = density of the slurry, g/cm^3
ρ_p = density of a spherical particle, g/cm^3
μ_o = viscosity of water, g/cm·s
μ_m = viscosity of the slurry, g/cm·s
μ_t = turbulent viscosity, g/cm·s
ν = kinematic viscosity, cm^2/s
η = dimensionless vorticity
Ψ = dimensionless stream function
Ω = dimensionless angular spin velocity

Literature Cited

Bhattacharyya, P., "Theoretical Study of the Flow Field inside a Hydrocyclone with Vortex Finder Diameter Greater than that of Apex Opening, I. Laminar Case, II. Turbulent Case," *Appl. Sci. Res.*, **36**, 197 (1980).
Bloor, M. I. G., and D. B. Ingham, "Theoretical Investigations of the Flow in a Conical Hydrocyclone," *Trans. Instn. Chem. Eng.*, **51**, 36 (1973).
Bloor, M. I. G., and D. B. Ingham, "Turbulent Spin in a Cyclone," *Trans. Instn. Chem. Eng.*, **53**, 1 (1975a).
Bloor, M. I. G., and D. B. Ingham, "The Leakage Effect in the Industrial Cyclone," *Trans Instn. Chem. Eng.*, **53**, 7 (1975b).
Bloor, M. I. G., and D. B. Ingham, "The Flow in Industrial Cyclones," *J. Fluid. Mech.*, **178**, 507 (1987).
Boysan, F., W. H. Ayers, and J. Swithenbank, "A Fundamental Mathematical Modelling Approach to Cyclone Design," *Trans. Instn. Chem. Eng.*, **60**, 222 (1982).
Bradley, D., and D. J. Pulling, "Flow Patterns in the Hydraulic Cyclone and Their Interpretation in Terms of Performance," *Trans. Instn. Chem. Eng.*, **37**, 34 (1959).
Brayshaw, M. D., "The Sharpening of the Hydrocyclone Efficiency Curve by Modification of the Flow Field Vorticity Function Using a Numerical Model," PhD Thesis, Univ. of Natal, Durban, S. Africa (1978).
Dabir, B., and C. A. Petty, "Laser Doppler Anemometry Measurements of Tangential and Axial Velocities in a Hydrocyclone Operating without an Air Core," *Proc. Int. Conf. on Hydrocyclones,* 15 (1984).
Driessen, M. G., "Theory of Flow in a Cyclone," *Rev. L'industrie Min. Spl.*, 449 (1951).
Frankel, S. P., "Convergence Rates of Iterative Treatment of Partial Differential Equations," *Math. Tables and Other Aids to Comp.*, **4**, 65 (1950).
Gourlay, A. R., "Hopscotch: A Fast Second-Order Partial Differential Equation Solver," *J. Inst. Maths. Applics.*, **6**, 375 (1970).
Gu, F., and W. Li, "Measurement and Study of Velocity Field in Various Cyclones by Use of Laser Doppler Anemometry," *Proc. Int. Conf. on Hydrocyclones,* 65 (1987).
Heiskanen, K., A. Vesanto, and H. Eronen, "A High Performance Hydrocyclone Design—The Twin Vortex Cyclone," *Proc. Int. Conf. on Hydrocyclones,* 263 (1987).
Hsieh, K. T., "Phenomenological Model of the Hydrocyclone," PhD Thesis, Univ. of Utah (1988).
Hsieh, K. T., and K. Rajamani, "Phenomenological Model of the Hydrocyclone: Model Development and Verification for Single-Phase Flow," *Int. J. Min. Proc.*, **22**, 223 (1988).
Kelsall, D. F., "A Study of the Motion of Solid Particle in a Hydraulic Cyclone," *Trans. Instn. Chem. Eng.*, **30**, 87 (1952).
Knowles, S. R., D. R. Woods, and I. A. Feuerstein, "The Velocity Distribution within a Hydrocyclone Operating without an Air Core," *Can. J. Chem. Eng.*, **51**, 262 (1973).
Laverack, S. D., "The Effect of Particle Concentration on the Boundary Layer Flow in a Hydrocyclone," *Trans. Instn. Chem. Eng.*, **58**, 33 (1980).
Lilge, E. O., "Hydrocyclone Fundamentals," *Trans. Inst. Min. and Met.*, **71**, 285 (1962).
Lilley, D. G., "Swirl Flows in Combustion: A Review," *AIAA J.*, **15**(8), 1063 (1977).
Morsi, Y. S. M., and B. R. Clayton, "Determination of Principal Characteristics of Turbulent Swirling Flow along Annuli," *Int. J. Heat Fluid Flow*, **7**, 208 (1986).
Ohashi, H., and S. Maeda, "Motion of Water in a Hydraulic Cyclone," *Chem. Eng. Japan*, **22**, 200 (1958).
Okhio, C. B., H. P. Horton, and G. Langer, "The Calculation of Turbulent Swirling Flow through Wide Angle Conical Diffusers and the Associated Dissipative Losses," *Int. J. Heat Fluid Flow*, **7**, 37 (1986).
Pericleous, K. A., N. Rhodes, and G. W. Cutting, "A Mathematical Model for Predicting the Flow Field in a Hydrocyclone Classifier," *Proc. Int. Conf. on Hydrocyclones,* 27 (1984).
Rietema, K., and H. J. Krajenbrink, "Theoretical Derivation of Tangential Velocity Profiles in Flat Vortex Chamber—Influence of Turbulence and Wall Friction," *Appl. Sci. Res.*, Sec. A, **8**, 177 (1959).
Rietema, K., "Performance and Design of Hydrocyclones: I. General

Considerations; II. Pressure Drop in the Hydrocyclone; III. Separating Power of the Hydrocyclone; IV. Design of Hydrocyclones," *Chem. Eng. Sci.*, **15**, 298 (1961).
Rietema, K., "Liquid-Solids Separation in a Cyclone—The Effect of Turbulence on Separation," *Instn. Chem. Eng.*, London, 275 (1962).
Rhodes, N., K. A. Pericleous, and S. N. Drake, "The Prediction of Hydrocyclone Performance with a Mathematical Model," *Proc. Int. Conf. on Hydrocyclones,* 51 (1987).
Roache, P. J., *Computational Fluid Dynamics,* Hermosa Publishers (1972).
Rodi, W., "Examples of Turbulence Model for Incompressible Flows," *AIAA J.*, **20**(7), 872 (1982).
Sloan, D. G., P. J. Smith and L. D. Smoot, "Modeling of Swirl in Turbulent Flow Systems," *Prog. Energy Combust. Sci.*, **12**, 163 (1986).
Syred, N., and J. M. Beér, "Combustion in Swirling Flows: A Review," *Combust. and Flame,* **23**, 143 (1974).
Tarjan, G., discussion on "Hydrocyclone Fundamentals," by E. O. Lilge, *Trans. Inst. Min. and Met.*, **71**, 539 (1962).
Upadrashta, K. R., V. J. Ketcham, and J. D. Miller, "Tangential Velocity Profile for Pseudoplastic Power-Law Fluids in the Hydrocyclone—a Theoretical Derivation," *Int. J. Min. Proc.*, **20**, 309 (1987).
Young, D., "Iterative Methods for Solving Partial Difference Equations of Elliptic Type," *Trans. Amer. Math. Soc.*, **76**, 92 (1954).

Manuscript received Sept. 13, 1990, and revision received Mar. 21, 1991.